Korean J. Chem. Eng., 37(11), 1999-2010 (2020)
DOI: 10.1007/s11814-020-0602-6

pISSN: 0256-1115
eISSN: 1975-7220

Adsorption isotherms and kinetics for the removal of cationic dye by *Cellulose*-based adsorbent biocomposite films

Noppon Somsesta*, Chaichana Piyamawadee*, Viboon Sricharoenchaikul, and Duangdao Aht-Ong*,***,†**

*Department of Materials Science, Faculty of Science, Chulalongkorn University, Bangkok, 10330, Thailand
**Department of Environmental Engineering, Faculty of Engineering, Chulalongkorn University, Bangkok, 10330, Thailand
***Center of Excellence on Petrochemical and Materials Technology, Chulalongkorn University, Bangkok, 10330, Thailand
(*Received 12 February 2020 • Revised 1 June 2020 • Accepted 4 June 2020*)

Abstract−Various fillers (commercial, nipa palm, sisal activated carbon, zeolite) were incorporated with regenerated cellulose matrix that dissolved using lithium chloride/N, N-dimethylacetamide solution. The biosorbent films were successfully prepared via solution casting and then characterized by Fourier transform infrared spectrometer (FTIR), X-ray Diffractometer (XRD), thermogravimetric analyzer (TGA), and scanning electron microscope (SEM). The biocomposite films with embedded commercial activated carbon exhibited the largest adsorption capacity of methylene blue (146.81 mg g^{-1}). Although the adsorption ability of the nipa palm and sisal activated carbon biocomposite was lower than the commercial activated carbon biosorbent film, both nipa palm and sisal activated carbon still could potentially be used as an alternative filler for cationic dye removal. On the contrary, zeolite had low adsorption efficiency owing to its morphology. The equilibrium adsorption experiment revealed that the Langmuir isotherm model best fitted the biocomposite films with commercial and sisal activated carbon, whereas the Freundlich adsorption model suited the biosorbent films with nipa palm activated carbon and zeolite than other models. The kinetics results of adsorption for all biocomposite films were well described using a pseudo-second-order kinetic model. The cellulose/activated carbon films would be promisingly utilized as a biosorbent for treatment of dye-contaminated wastewater.

Keywords: Cellulose Biocomposite Film, Isotherm, Activated Carbon, Methylene Blue Adsorption, Kinetic

INTRODUCTION

Dyes, organic compounds that are soluble in water, have been extensively utilized in several industries, such as printing, textile, rubber, plastic, cosmetic, food, leather, and pharmaceutical [1]. Therefore, large amounts of dye-contaminated wastewater from these manufacturing has been emitted into the environment, which could lead to dramatic water pollution if the dye effluents are directly released or not treated with the proper methods [2]. This wastewater could cause harm to human and aquatic organisms owing to the toxicity and carcinogenicity of dyes [3]. Hence, the treatment of wastewater has become a highly active research topic. Various processes (i.e., membrane filtration, ion exchange, biological treatment, chemical precipitation, coagulation, catalytic degradation, adsorption) have been proposed and developed for removal of contaminants from polluted water [4]. Among several techniques, adsorption is broadly used due to its simplicity and effectiveness [5,6]. Although various types of adsorbents, such as activated carbon, zeolite, clay, chitosan, are available and used in many purposes, activated carbon is commonly used to adsorb pollutants from air and water due to its huge pore size, large pore volume, and extremely high surface area [7-9]. In addition, many studies have been conducted to enhance adsorption efficiency.

Activated carbon, a black solid carbon substance, can be produced by carbonization of biomass at elevated temperature under inert condition, a process called "pyrolysis" [10]. Recently, different kinds of biomass were used as precursor to make activated carbon [11-13]. To optimize the activated carbon adsorption performance, several researchers have investigated the effect of pyrolysis conditions; for example, retention time [14,15], pyrolysis temperature [16,17], heating rate [18,19], and pressure [20] on specific surface areas and porous characteristic. However, activated carbon and many commercial absorbents are usually utilized in the form of powder, which makes it difficult to recover and regenerate. This restricted their practical application because if the powdered adsorbents were directly used and remained in the environment, they would end up as the secondary waste. It is important to find a suitable matrix for implantation that could prevent the production of additional pollutants.

Cellulose, a renewable resource that consists of repeated glucose units bonded together by β(1-4) glycosidic bonds [21], has gained increasing attention because it is a low-cost precursor, environmentally friendly material, biodegradable substance, with great resistance to common organic solvents [22,23]. Over the past few years, the dissolution of cellulose has been achieved using lithium chloride/N, N-dimethylacetamide (LiCl/DMAc) solvent and there have been several works that successfully prepared the cellulose-based composite [24-26]. Hence, in this study, we aimed to immobilize the fillers (commercial, nipa palm, sisal activated carbon, zeolite) into the cellulose matrix and fabricate the cellulose biocomposite film that could remove dyes from aqueous solution which can be easily recovered after being used. To the best of our knowledge, the

†To whom correspondence should be addressed.
E-mail: duangdao.a@chula.ac.th

comparative study of adsorption of dyes onto the biosorbent films with different fillers has not been conducted. The cellulose solution was combined with various fillers, and the biocomposite films were successfully produced by solution casting method. The biocomposite films were then characterized using FTIR, SEM, XRD, and TGA. The adsorption isotherms and kinetics were investigated to gain comprehensive information on the sorption behavior of the biocomposite films. In addition, regeneration studies of the biocomposite films were also carried out to evaluate the reusability of these adsorbents and make them sustainable and economical towards the environment.

MATERIAL AND METHODS

1. Materials and Chemicals

Sisal fiber was acquired from agricultural Hubkapong Cooperatives, Phetchaburi, Thailand. Nipa palm activated carbon (npac) was sourced locally. Commercial activated carbon (cac) and zeolite Y (zy) were purchased from Sigma-Aldrich. Sodium hydroxide (NaOH) and N, N-dimethylacetamide (DMAc) were obtained from RCI Labscan Limited, Samut Sakhon, Thailand. Hydrogen peroxide (H_2O_2), lithium chloride (LiCl), potassium hydroxide (KOH), and other chemicals were of analytical grade and used as received.

2. Preparation of Sisal Activated Carbon

Sisal activated carbon (sac) was prepared via pyrolysis of sisal fiber according to the Somsesta and Aht-Ong work [27]. The carbonization proceeded at 700 °C with 2 : 1 ratio of chemical activating reagent (KOH)/sisal fiber under nitrogen flow. The received activated carbon was washed with distilled water and subsequently dried overnight in oven at 60 °C.

3. Filler Characterization

The adsorption capability of all fillers (cac, npac, sac, zy) was determined by removal efficiency of methylene blue from aqueous solution. The experiment was conducted via spreading the fillers into the 50 ml of 500 mg L^{-1} methylene blue dye solution for 24 hr. The samples were then centrifuged to separate spent fillers. The remaining methylene blue concentration in the supernatant was measured using an ultraviolet-visible spectroscopy in accordance with methylene blue calibration curve at the maximum wavelength (664 nm). The dye adsorption capacity was estimated using the equation shown below [28].

$$Q_t = \frac{(C_0 - C_t)V}{M} \quad (1)$$

where Q_t is the quantity of dye molecules adsorbed by the fillers (mg/g), C_0 is the initial methylene blue concentration (mg/L), C_t is the remaining methylene blue concentration at time t (mg/L), V is volume of solution (L), and M is fillers weight (g). Scanning electron microscopy (SEM) under the accelerating voltage 15 kV was utilized to explore the morphology and surface details of the fillers. Prior to the examination, sputtering technique was applied to coat the fillers with gold to prevent electron charging on the surface of specimens. The samples were then subjected to Fourier transform infrared spectroscopy (FTIR) for investigation of chemical structure. The analysis was carried out using KBr pellet method, and the spectra were recorded in the range from 4,000-400 cm^{-1} at 8 cm^{-1} resolution. X-ray diffractometry (XRD) was used to analyze the crystalline composition under Cu Kα radiation (λ=0.1540 nm) at 40 kV and 40 mA. The diffractograms were collected in the angle between 2θ= 5 to 60° at a scanning speed of 2° min^{-1}. Thermogravimetric analysis was performed to examine thermal characteristic of the samples. Here, 10±1 mg of specimens was heated from ambient temperature to 900 °C at a heating rate of 10 °C min^{-1} under nitrogen flow.

4. Biocomposite Film Preparation and Characterization

The sisal cellulose was extracted from sisal fiber by delignification using sodium hydroxide, and then bleached by sodium hydroxide/30% hydrogen peroxide solution. The obtained sisal cellulose was subsequently dissolved using LiCl/DMAc solution, and further used as a matrix for the biocomposite film.

The fillers (3 g) were mixed with cellulose solution (100 ml), and the activated carbon was evenly distributed throughout the mixture by sonification and magnetic stirring, respectively. The mixture was then spread over a glass mould, and held at room temperature for 8 hr. The composite gel was subsequently cleaned using distilled water and isolated under ambient condition until the biocomposite films were fully dried. The composite films were labeled as cacc, npacc, sacc, and zyc, according to the fillers that embedded in the biosorbent.

The surface structure as well as morphology of the samples were investigated using scanning electron microscopy (JSM 6400, JEOL, Tokyo, Japan). The film surface and cross-section were covered with gold before the testing. The chemical composition was investigated by Fourier transform infrared spectrometer with attenuated total reflectance (ATR) method. The infrared spectra ranged between 4,000-400 cm^{-1} at 8 cm^{-1} scan rate. The crystalline structure was characterized by X-Ray diffractometer with Cu Kα radiation under accelerating voltage of 40 kV and a current of 40 mA. The scanning range was recorded from 2θ=5 to 60°, with rate of 2° min^{-1}. The thermal characteristic was examined using thermogravimetric analyzer where samples were heated from room temperature to 900 °C at a heating rate of 10 °C min^{-1} under nitrogen atmosphere.

5. Adsorption Isotherms Study

Cationic methylene blue dye was also used in the adsorption experiment. The biocomposite films were cut into 1×1 cm^2 parts and dried overnight before use. To initiate the testing, the samples were dropped into 50 ml methylene blue solution at concentration of 20, 40, 60, 80, 100 mg L^{-1} for 24 hr. Adsorption efficiency of the biocomposite films was determined by a UV-vis spectrophotometer and calculated using Eq. (1).

The Langmuir (Eq. (2)) and Freundlich (Eq. (3)) adsorption isotherm models [29] were applied to the experimental data, and the relevant equations are shown below:

$$\frac{C_{eq}}{Q_{eq}} = \frac{1}{k_L Q_{max}} + \frac{C_{eq}}{Q_{max}} \quad (2)$$

where Q_{eq} (mg g^{-1}) is the amount of methylene blue adsorbed on the films at equilibrium, C_{eq} (mg L^{-1}) is the methylene blue concentration in solution at equilibrium, k_L (L mg^{-1}) is the equilibrium constant of Langmuir isotherm, and Q_{max} (mg g^{-1}) is the maximum monolayer coverage capacity of methylene blue onto the

adsorbents. The values of $1/k_L$ Q_{max} and $1/Q_{max}$ can be calculated from the intercept and slope of linear regression plots of C_{eq}/Q_{eq} versus C_{eq} for Eq. (2).

$$\ln Q_{eq} = \ln k_F + \frac{1}{n}\ln C_{eq} \quad (3)$$

where k_F (mg g^{-1}) is the adsorption equilibrium constant of Freundlich isotherm and 1/n is the Freundlich characteristic constants corresponding to adsorption intensity and adsorption capacity of the adsorbents. The values of $\ln k_F$ and 1/n can be estimated from the intercept and slope of linear regression plots between $\ln Q_{eq}$ and $\ln C_{eq}$ for Eq. (3).

The experimental data were also fitted to the Temkin (Eq. (4)) and Dubinin-Raduskevich (Eq. (5)) models [30], using the equations presented below:

$$Q_{eq} = \frac{RT}{bT}\ln kT + \frac{RT}{bT}\ln C_{eq} \quad (4)$$

$$\ln Q_{eq} = \ln Q_D - BD\varepsilon^2 \quad (5)$$

where Q_{eq} (mg g^{-1}) is the amount of methylene blue adsorbed on the films at equilibrium, C_{eq} (mg L^{-1}) is the methylene blue concentration in solution at equilibrium, kT (L g^{-1}) is the Temkin adsorption equilibrium constant related to the maximum binding energy, R (J mol^{-1} K^{-1}) is the gas constant, T (K) is absolute temperature and bT (J mol^{-1}) is the variation in adsorption energy related to the enthalpy of reaction. The values of $\frac{RT}{bT}\ln kT$ and $\frac{RT}{bT}$ can be evaluated from the intercept and slope of linear regression plots of Q_{eq} versus C_{eq} for Eq. (4).

For Eq. (5), where Q_D (mg g^{-1}) is Dubinin-Radushkevich isotherm constant corresponding to the degree of adsorption by the adsorbent, BD (mol^2 kJ^{-2}) is Dubinin-Radushkevich isotherm constant related to the adsorption energy, ε is the Polanyi potential energy which can be calculated using equation $\varepsilon = RT\ln(1+(1/C_{eq}))$, where R (J mol^{-1} K^{-1}) is the gas constant, and T (K) is the absolute temperature. The values of $\ln Q_D$ and BD can be determined from the intercept and slope of linear regression plots between Q_{eq} and ε^2. Furthermore, E is the energy parameter that provides the data related to adsorption characteristic, as shown in Eq. (6).

$$E = \frac{1}{\sqrt{2BD}} \quad (6)$$

6. Adsorption Kinetics Study

The kinetic experiments were operated by immersing the biocomposite film (1×1 cm^2) in methylene blue dye solution at concentration of 40 mg L^{-1} for fixed time intervals. After removal of a specimen, the remaining methylene blue concentration was examined by a UV-vis spectrophotometer.

The kinetics data were then fitted to Lagergren pseudo-first-order, pseudo-second-order, Elovich models [31], as shown in Eq. (7)-(9), respectively.

$$\frac{1}{Q_t} = \left(\frac{k_1}{Q_1}\right)\left(\frac{1}{t}\right) + \frac{1}{Q_1} \quad (7)$$

where Q_t (mg g^{-1}) is the amount of methylene blue adsorbed on the films at time t, k_1 (1 min^{-1}) is the rate constant of pseudo-first-order, Q_1 (mg g^{-1}) is the maximum amount of dyes adsorbed onto the adsorbents, and t (min) is the uptake time. The values of $1/Q_1$ and k_1/Q_1 can be estimated from the intercept and slope of linear regression plots of $1/Q_t$ versus 1/t for Eq. (7).

$$\frac{t}{Q_t} = \frac{1}{k_2 Q_2^2} + \frac{t}{Q_2} \quad (8)$$

where k_2 (g mg^{-1} min^{-1}) is the rate constant of pseudo-second-order and Q_2 (mg g^{-1}) is the maximum amount of dyes adsorbed onto the adsorbents. The values of $1/k_2Q_2^2$ and $1/Q_2$ can be calculated from the intercept and slope of linear regression plots between t/Q_t and t for Eq. (8).

$$Q_t = \frac{1}{\beta}\ln\alpha\beta + \frac{1}{\beta}\ln t \quad (9)$$

where β (g mg^{-1}) is the extent of surface coverage and activation energy for the adsorption process and α (mg g^{-1} min^{-1}) is the initial adsorption rate constant. The values of $\frac{1}{\beta}\ln\alpha\beta$ and $1/\beta$ can be determined from the intercept and slope of linear regression plots of Q_t versus lnt for Eq. (9).

Moreover, an expanded study on adsorption kinetics was conducted with the fitting of kinetics data to the intraparticle diffusion model [32], using the following equation:

$$Q_t = k_P t^{1/2} + C \quad (10)$$

where Q_t (mg g^{-1}) is the amount of methylene blue adsorbed on the films at time t, k_P (mg g^{-1} $min^{-1/2}$) is the rate constant of intraparticle diffusion, t (min) is the time of the adsorption process, and C (mg g^{-1}) is the constant which corresponded to the thickness of boundary layer. The values of C and k_P can be evaluated from the intercept and slope of linear regression plots between Q_t and $t^{1/2}$ for Eq. (10).

7. Reusability Study

The biocomposite films were recycled by immersing the 1×1 cm^2 film specimens into the dye solution containing 50 ml of 20 mg L^{-1} of methylene blue for 24 hr. After the biocomposite films were recovered, they were then treated with 0.1 M NaOH solution for 9 hr to elute methylene blue dye from their surfaces. The film specimens were subsequently rinsed with deionized water to get rid of any remaining alkaline before the next run. Adsorption-desorption was performed for five consecutive runs using the same film under the same operating conditions. The % decolorization of the biocomposite films was calculated as follows:

$$\text{Decolorization (\%)} = \left(\frac{C_0 - C_t}{C_0}\right) \times 100 \quad (11)$$

where C_0 (mg L^{-1}) is the initial concentration of methylene blue in solution, C_t (mg L^{-1}) is the concentration of methylene blue in solution at time t.

RESULTS AND DISCUSSION

1. Characterization of Fillers

The morphology of fillers was investigated by SEM, and dis-

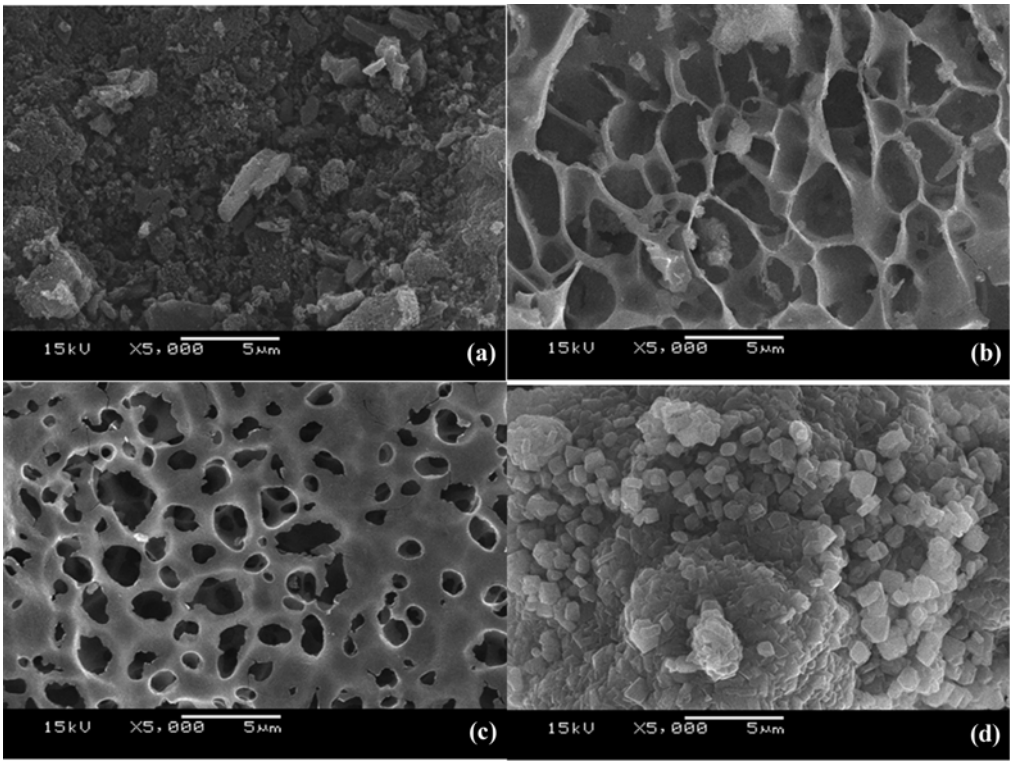

Fig. 1. SEM image of (a) commercial activated carbon (cac), (b) nipa palm activated carbon (npac), (c) sisal activated carbon (sac), and (d) zeolite Y (zy).

Table 1. Methylene blue adsorption of various fillers

Filler	Methylene blue adsorption capacity (mg g^{-1})
commercial-ac	421.74
nipa palm-ac	273.38
sisal-ac	181.21
zeolite Y	34.07

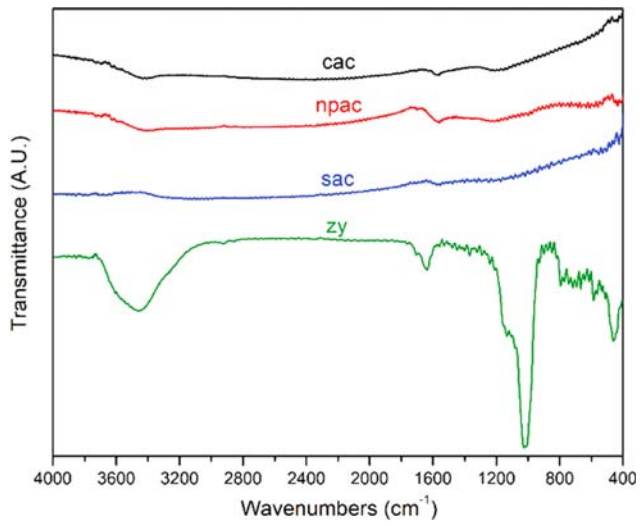

Fig. 2. FTIR spectra of activated carbon (cac), nipa palm activated carbon (npac), sisal activated carbon (sac), and zeolite Y (zy).

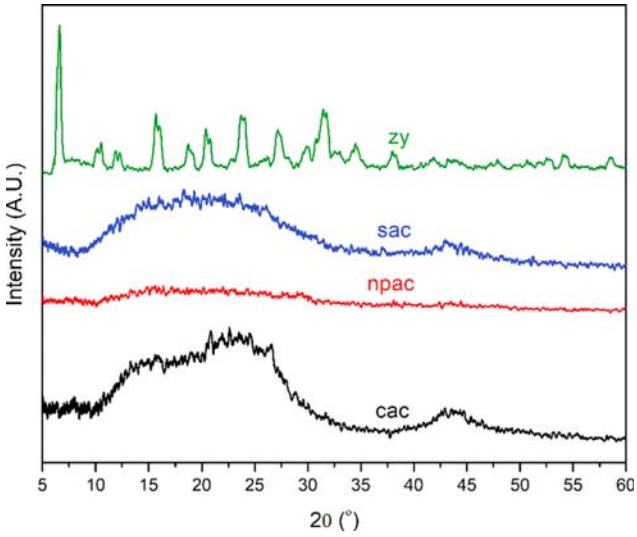

Fig. 3. XRD patterns of activated carbon (cac), nipa palm activated carbon (npac), sisal activated carbon (sac), and zeolite Y (zy).

played in Fig. 1(a), (b), (c), (d). From the figures, highly and well-ordered porous structure was observed in commercial activated carbon, nipa palm activated carbon, and sisal activated carbon, respectively. This was ascribed to their high adsorption amount of dye as listed in Table 1. Even zeolite Y had a high specific surface area [33]; methylene blue was hardly adsorbed onto zeolite due to its porous dimension. At the same resolution, cubic stacking was

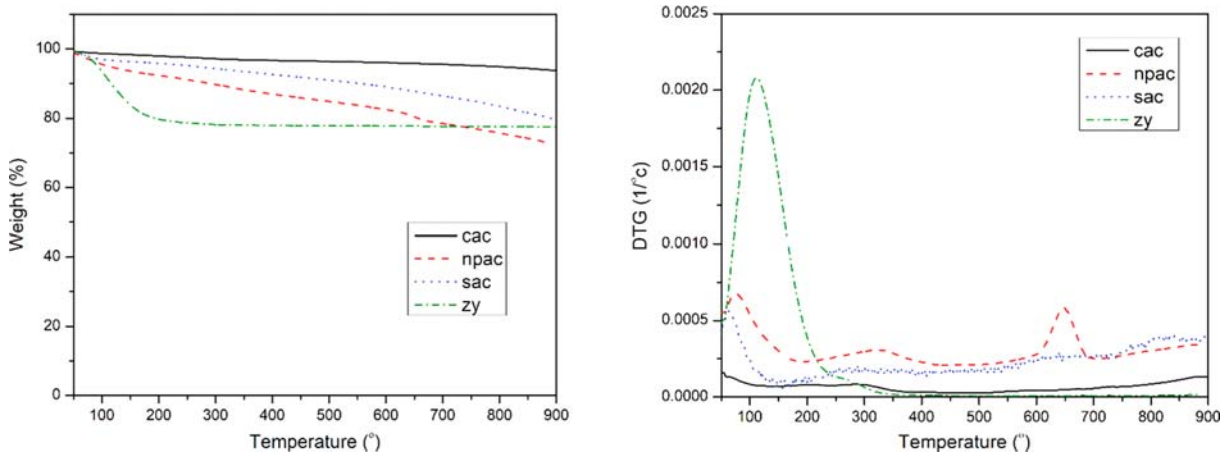

Fig. 4. TGA and DTG curves of activated carbon (cac), nipa palm activated carbon (npac), sisal activated carbon (sac), and zeolite Y (zy).

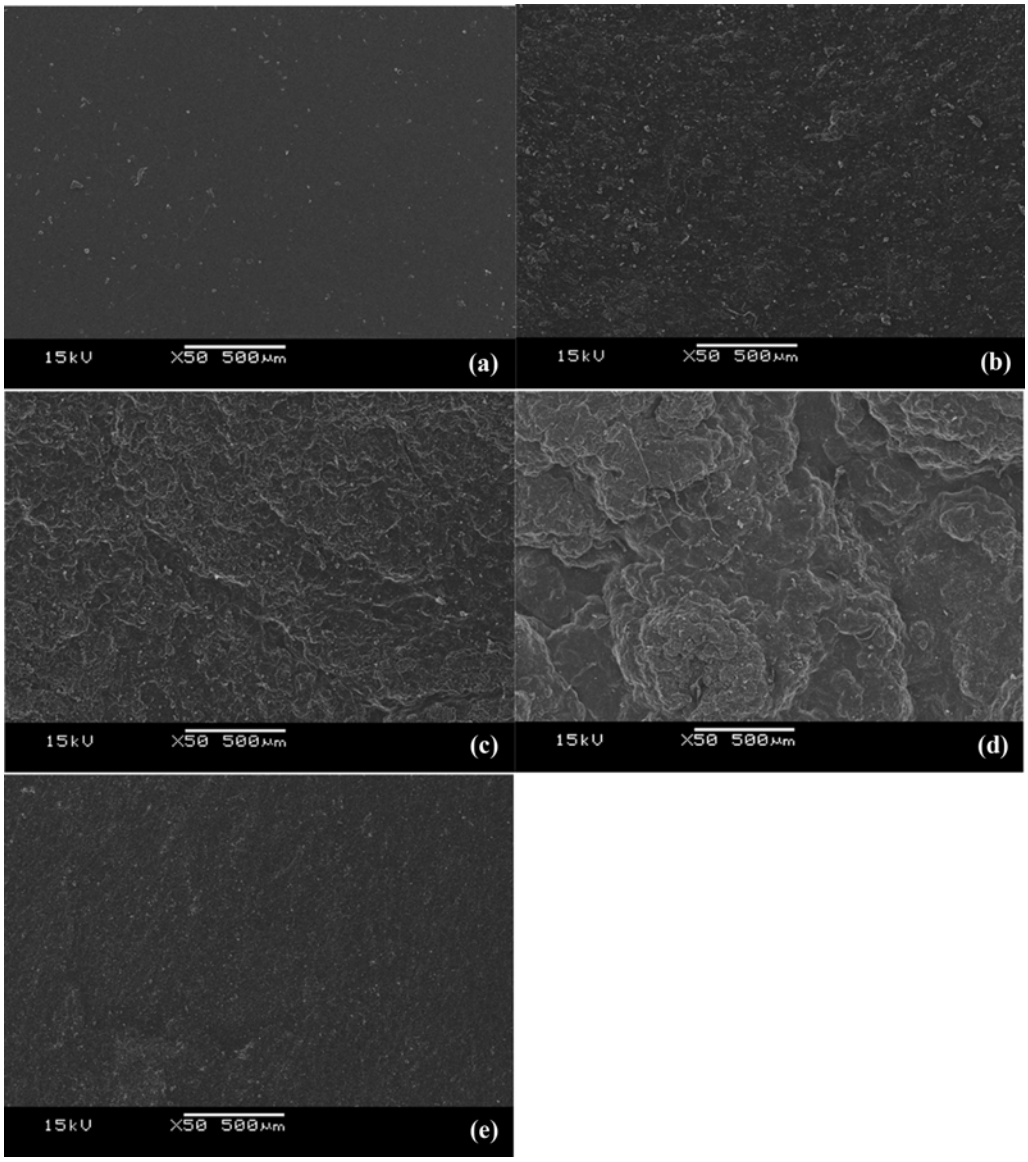

Fig. 5. SEM surface images of (a) cellulose neat, (b) commercial activated carbon composite (cacc), (c) nipa palm activated carbon composite (npacc), (d) sisal activated carbon composite (sacc), and (e) zeolite Y composite (zyc) films.

observed in Fig. 1(d) and there were no apparent pores detected on the zeolite surface. For this reason, the filler which had the lowest adsorption capacity to remove dye in this study was zeolite.

The chemical structure of fillers was then examined by FTIR. As shown in Fig. 2 the spectra of cac, npac, and sac were broad throughout the line, indicating that the functional groups of these fillers were eliminated after pyrolysis process.

The spectrum of zeolite revealed the band at the region 3,500 cm^{-1} and 1,650 cm^{-1}, corresponding to O-H stretching of surface hydroxylic group and lattice water molecules, respectively. The intense peak at 1,000 cm^{-1} was owing to Si-O/Al-O stretching [34]. X-ray diffraction was used to study the crystalline composition of fillers and the diffractograms are presented in Fig. 3. The broad peaks at 2θ=43° and 25° of commercial-ac and sisal-ac fillers correspond to the occurrence of turbostratic structure of disorganized carbon [35].

Meanwhile, xrd pattern of nipa palm-ac indicated the fully amorphous structure of this filler. The standard peaks of zeolite y were observed at 2θ=6, 10, 12, 16, 19, 20, 24, 27, 31 and 32°, respectively [36].

The thermal analysis curve of fillers was examined and shown in Fig. 4. The commercial activated carbon exhibited the highest thermal stability, the total weight loss was approximately 6.26 wt%, mostly from the loss of moisture. In case of nipa palm-ac and sisal-ac, the total weight loss was about 27.54 and 20.36 wt%, respectively. The degradation was divided into two stages; the first was due to the evaporation of water which occurred in the range of 50 to 180 °C. The later stage proceeded between 180 and 900 °C which was attributed to the destruction of the aromatic organic substances like lignin [37]. A thermogram of zeolite displayed the total weight loss of approximately 22.53 wt%. It could be ascribed to the elimination of water that took place in the range between 50 to 200 °C [36].

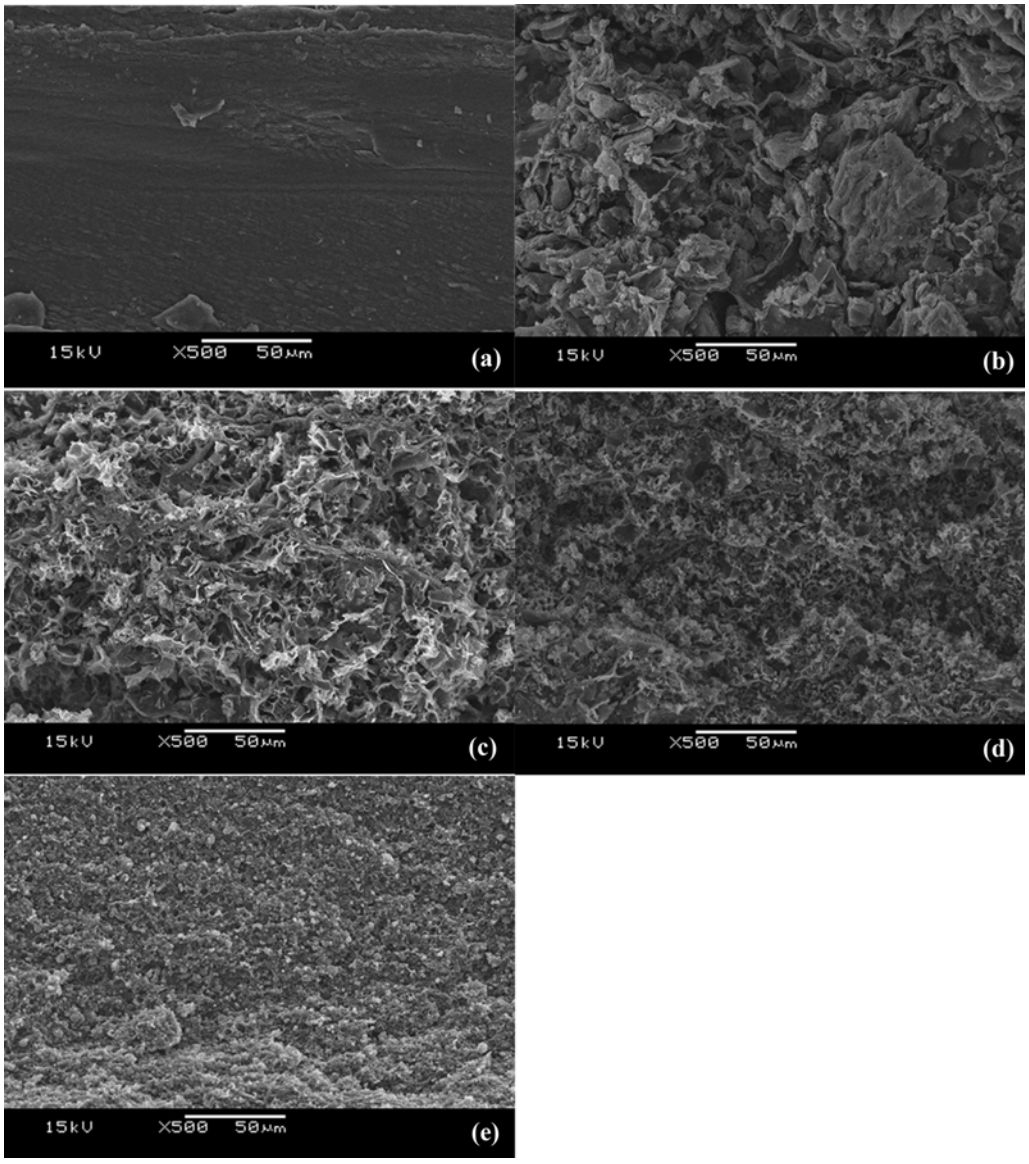

Fig. 6. SEM images of cross-section for (a) cellulose neat, (b) commercial activated carbon composite (cacc), (c) nipa palm activated carbon composite (npacc), (d) sisal activated carbon composite (sacc), and (e) zeolite Y composite (zyc) films.

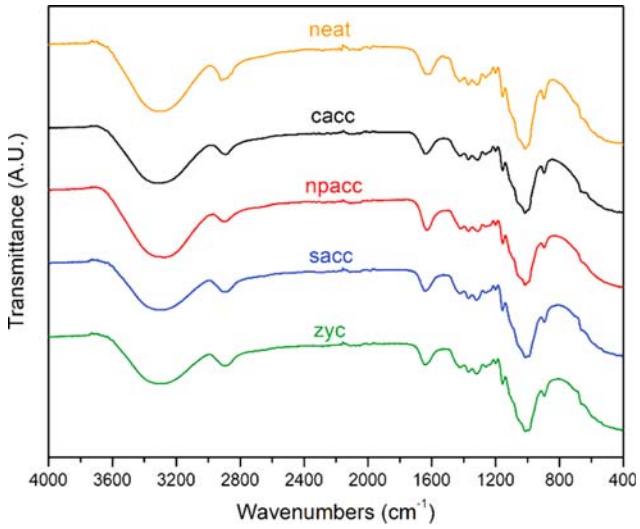

Fig. 7. FTIR spectra of cellulose neat, commercial activated carbon composite (cacc), nipa palm activated carbon composite (npacc), sisal activated carbon composite (sacc), and zeolite Y composite (zyc) films.

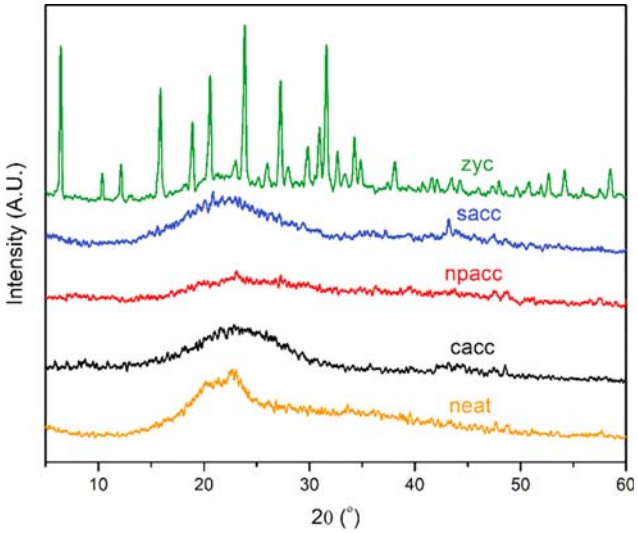

Fig. 8. XRD patterns of cellulose neat, commercial activated carbon composite (cacc), nipa palm activated carbon composite (npacc), sisal activated carbon composite (sacc), and zeolite Y composite (zyc) films.

2. Characterization of Biocomposite Films

The morphology of composite films prepared from different fillers is exhibited in Fig. 5. A flat surface of cellulose neat film is displayed in Fig. 5(a). A rough surface was observed when various fillers were added as shown in Figs. 5(b), (c), (d), (e). The SEM images of cross-section also indicate that cellulose neat film had a smooth surface and became rougher after the fillers were embedded. Figs. 6(b), (c), (d), (e) reveal that the fillers are well spread over the cross-sectional surface of biocomposite films. This rough surface could enhance the adsorption capacity of biocomposite films because it would act as adsorption sites and robustly transport dye molecules to deposit when the adsorption takes place [31].

The chemical composition of the biocomposite films was investigated via FTIR, and the acquired spectra are displayed in Fig. 7, indicating no apparent changes on the chemical structure of the biocomposite films.

All spectra contained the typical peaks of cellulose, consisting of stretching vibrations of the hydroxyl group in glucose units, C-H stretching vibrations of all hydrocarbon component in glucose units, and C-H bending vibrations in cellulose at 3,331 cm^{-1}, 2,894 cm^{-1}, and 1,428 cm^{-1}, respectively [38]. In addition, C-O-C pyranose ring vibration appeared at 1,069 cm^{-1} and a band near 1,647 cm^{-1} was corresponding to the water hydration (H-O-H bending of adsorbed water) [39].

The XRD analysis was used for determining the crystalline structure of composite films, and the diffractograms is presented in Fig. 8. The diffraction pattern of neat film exhibited a band at 2θ=20 and 22°, corresponding to the [002], and [10$\bar{1}$] lattice planes of cellulose II, which were the main diffraction pattern of cellulose II or regenerated cellulose [40].

When the activated carbons were added, the region between 2θ= 20 and 24° in the diffractograms of composite films was broad-

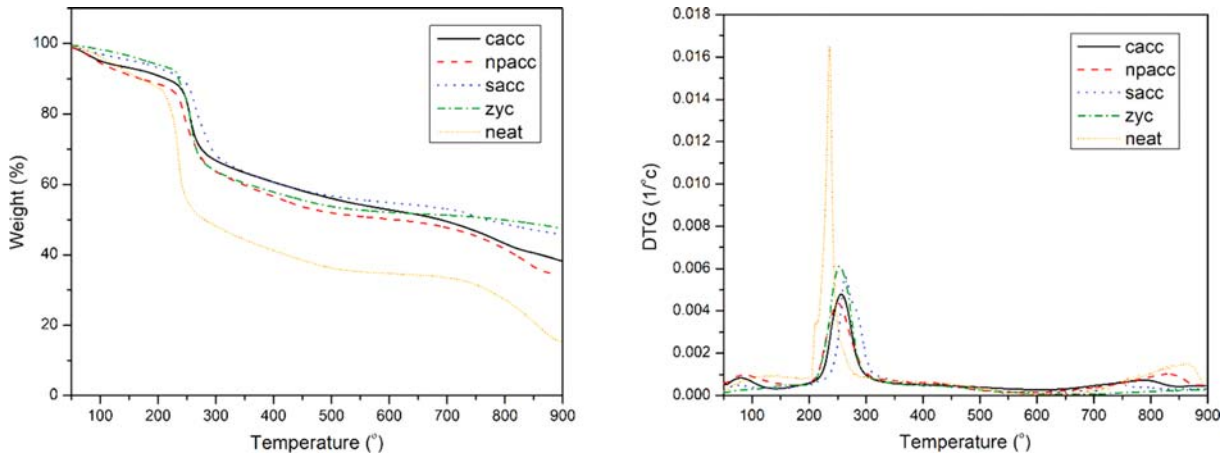

Fig. 9. TGA and DTG curves of cellulose neat, commercial activated carbon composite (cacc), nipa palm activated carbon composite (npacc), sisal activated carbon composite (sacc), and zeolite Y composite (zyc) films.

ened, implying that the recrystallization of regenerated cellulose was probably prevented. Nevertheless, this was a favorable change since liquid or gas would easily be transported through loose or disordered network like amorphous structure [24]. For this reason, an increment in amorphous would promote the adsorption process and enhance the adsorption ability of the composite films. Meanwhile, the diffractogram of zeolite Y composite film still maintained the zeolite pattern.

The thermal behavior of composite films was also studied. Fig. 9 displays TGA and DTG thermograms of the biocomposite films. The sisal-ac composite film had the highest thermal stability with total weight loss of approximately 54.39% at 900 °C, while the remaining weight of neat film was only 15.29% at the same temperature. Compared to the cellulose neat film, the onset degradation temperature of the biocomposite films was increased along with a reduction of total weight loss. Hence, it could be concluded that the insertion of fillers would enhance thermal stability for the composite films.

3. Adsorption Isotherm

Adsorption characteristics of methylene blue on the composite films were determined. Various isotherm models--Langmuir, Freundlich, Temkin, and Dubinin-Raduskevich--were used to describe the interaction between adsorbed molecules and the composite films. The adsorption capacity at equilibrium was investigated and presented in Fig. 10. The amount of dyes adsorbed increased at higher initial concentration for all films. This could be explained by the fact that higher initial dye concentration provides greater driving force to overcome the mass transfer resistance of the dye particles between the aqueous solution and the adsorbent surface and hence enhances the adsorption process [41]. As expected, commercial-ac composite showed the highest adsorption values among any composite films, approximately 146.81 mg g^{-1} since commercial-ac had the greatest adsorption capacity. Meanwhile, the addition of nipa palm-ac and sisal-ac could improve the methylene blue adsorption capacity from 30.28 to 123.58 and 103.66 mg g^{-1}, respectively. However, similar enhancement for zeolite composite was limited; this could be attributed to its surface morphology, as mentioned earlier.

The linearized Langmuir and Freundlich isotherm graphs are shown in Fig. S1. In addition, Table 2 presents the estimated Langmuir and Freundlich parameters, including correlation coefficient (R^2). In term of R^2, the results reveal that the isotherm data of commercial-ac composite, sisal-ac composite, and cellulose neat films are best fitted by Langmuir isotherm model, indicating the dye molecules were deposited on the films surface by monolayer adsorption in nature. Meanwhile, the experiment data of nipa palm-ac composite and zeolite composite could be described by Freundlich adsorption, implying that the methylene blue was adsorbed on the biocomposite films as a heterogeneous surface with multilayer sorption [42].

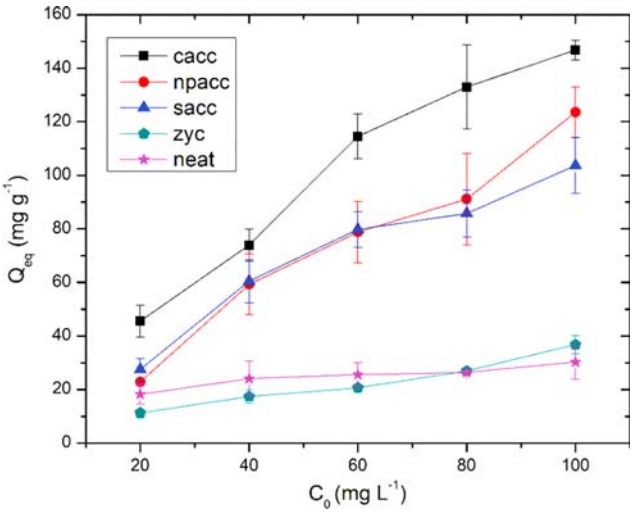

Fig. 10. Adsorption isotherm of methylene blue on cellulose neat, commercial activated carbon composite (cacc), nipa palm activated carbon composite (npacc), sisal activated carbon composite (sacc), and zeolite Y composite (zyc) films.

Moreover, the Langmuir monolayer maximum sorption capacity (Q_{max}) for commercial-ac composite, nipa palm-ac composite, sisal-ac composite, zeolite composite, and cellulose neat films was estimated as 158.35, 140.06, 110.35, 58.97, and 33.84 (mg g^{-1}), respectively. The Langmuir constant (k_L) is related to the energy of adsorption. High k_L constant indicates a greater affinity between the adsorbate and adsorption sites on the adsorbent surface [43]. Therefore, the attractive forces between dye molecules and commercial-ac composite were highest, while zeolite composite film was the lowest. In addition, the calculated Freundlich constant or 1/n could indicate the feasibility of the adsorption system. Here, $0.1<1/n\leq 0.5$, demonstrating the adsorption is favorable; $0.5<1/n\leq 1$, there is some difficulties in sorption process; $1/n>1$, the adsorption process is unfavorable [44]. The analyzed data show that the adsorption process was satisfactory except the zeolite composite film in which 1/n was approximately 0.58. Hence, some obstacles occurred

Table 2. Isotherm parameters for methylene blue adsorption onto neat and biocomposite films

	Langmuir			Freundlich			Temkin			Dubinin-Radushkevich (D-R)			
	Q_{max} (mg g^{-1})	k_L (L mg^{-1})	R^2	1/n	k_F (mg g^{-1})	R^2	bT (J mol^{-1})	kT (kJ mol^{-1})	R^2	BD (mol^2 kJ^{-2})	Q_D (mol^2 kJ^{-2})	E (J mol^{-1})	R^2
cacc	158.35	0.4638	0.9796	0.2754	63.616	0.9707	0.107	19.826	0.9151	5.5137×10^{-8}	114.9981	3.0114×10^{3}	0.7356
npacc	140.06	0.1426	0.9763	0.4405	26.050	0.9811	0.0973	2.361	0.9743	3.7117×10^{-7}	88.1413	1.1606×10^{3}	0.8680
sacc	110.35	0.2394	0.9917	0.3287	31.885	0.9668	0.133	5.255	0.9965	2.7819×10^{-7}	83.0373	1.3407×10^{3}	0.8972
zyc	58.97	0.01604	0.7519	0.5828	2.582	0.9559	0.206	0.182	0.8519	1.9929×10^{-5}	26.6404	1.5845×10^{2}	0.7190
neat	33.84	0.07351	0.9860	0.2665	9.157	0.9573	0.397	1.335	0.9538	1.4585×10^{-5}	27.7400	1.8519×10^{2}	0.8918

during the adsorption of zeolite composite, and resulted in low adsorption abilities for this composite film.

The isotherm plots of Temkin and Dubinin-Raduskevich models are displayed in Fig. S1. Corresponding calculated isotherm parameters and correlation coefficient are also listed in Table 2. According to the Temkin isotherm, when the heat of adsorption (bT) was less than 20 J mol^{-1}, the physisorption dominating chemisorption [45]. Therefore, the adsorption of all biocomposite films was governed by physisorption interaction. From the linear graph of Dubinin-Radushkevich isotherm, mean free energy of sorption per molecule of sorbate or E was determined. This was a useful factor that could predict the adsorption properties, hence it indicated that any biocomposite films in this study were associated with a physisorption as the E values for all films were lower than 8 kJ mol^{-1} [46].

4. Adsorption Kinetics

The objective of the adsorption kinetics study was to investigate the adsorption rate and mechanism. Various kinetics models--Lagergren pseudo-first-order, pseudo second-order, Elovich, and intraparticle diffusion--were applied to the experiment data. The plotting of adsorption capacity of the biocomposite films against contact time is presented in Fig. 11. Owing to the large availability of vacant surface sites, during the first 3 hrs (180 min), the dye molecule uptake rapidly occurred and was still increasing for several hours thereafter. The adsorption rate was then gradually decreased and almost reached equilibrium at 18 hrs (1,080 min). This could be attributed to the drastic reduction of the adsorption sites, and also due to the repulsive forces between methylene blue molecules adsorbed on the composite surface and those in aqueous solution. Finally, the adsorption equilibrium took place within 24 hrs (1,440 min) due to the saturation of the active sites, and therefore the adsorption capacity remained almost constant [5].

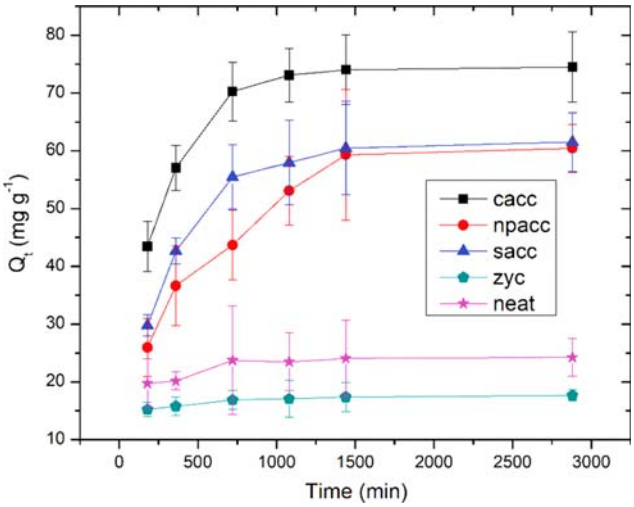

Fig. 11. Adsorption kinetic of methylene blue on cellulose neat, commercial activated carbon composite (cacc), nipa palm activated carbon composite (npacc), sisal activated carbon composite (sacc), and zeolite Y composite (zyc) films.

The linearized pseudo-first-order, pseudo-second-order, and Elovich kinetics graphs are shown in Fig. S2, and the parameters determined from these plots are listed in Table 3. The correlation coefficient or R^2 indicated that dye molecule adsorption for any films including cellulose neat film was following the pseudo-second-order kinetic model. This suggested that chemisorption was the rate-controlling step in adsorption system for all films, hence the sorption process associated with the valence forces through

Table 3. Kinetic parameters for methylene blue adsorption onto cellulose neat, commercial-ac composite, nipa palm-ac composite, sisal-ac composite, and zeolite composite films

	Pseudo-first-order Model			Pseudo-second-order Model			Elovich model		
	Q_1 (mg g^{-1})	k_1 (1 min^{-1})	R^2	Q_2 (mg g^{-1})	k_2 (g mg^{-1} min^{-1})	R^2	β (g mg^{-1})	α (mg g^{-1} min^{-1})	R^2
cacc	82.47	159.6853	0.9890	78.00	1.2016×10^{-4}	0.9989	0.0854	4.0422	0.8580
npacc	65.88	280.8693	0.9856	67.45	$4.9282\times10^{-}0^{-5}$	0.9958	0.0747	0.5614	0.9543
sacc	70.71	243.3039	0.9920	65.90	8.8191×10^{-5}	0.9984	0.0837	1.1400	0.8947
zyc	17.61	30.7195	0.9241	17.90	1.2883×10^{-3}	0.9999	1.0652	62410.8343	0.9563
neat	24.57	49.5236	0.8391	24.74	7.6998×10^{-4}	0.9997	0.5292	377.9266	0.8337

Table 4. Kinetic parameters of intraparticle diffusion model

	Intraparticle diffusion model								
	C_1 (mg g^{-1})	k_{P1} (mg/g^{-1} $min^{-1/2}$)	R_1^2	C_2 (mg g^{-1})	k_{P2} (mg/g^{-1} $min^{-1/2}$)	R_2^2	C_3 (mg g^{-1})	k_{P3} (mg/g^{-1} $min^{-1/2}$)	R_3^2
cacc	31.30	1.2409	0.8877	72.79	0.03185	1.000	-	-	-
npacc	9.55	1.3147	0.9893	56.54	0.07282	1.000	-	-	-
sacc	5.21	1.8963	0.9902	43.38	0.4486	0.9973	58.02	0.06483	1.0000
zyc	14.13	0.08971	0.9534	16.72	0.01752	1.000	-	-	-
neat	17.15	0.1955	0.8549	23.66	0.01091	1.0000	-	-	-

Table 5. Reusability studies for the adsorption-desorption cycles of methylene blue onto the biocomposite films

	% Decolorization at adsorption-desorption cycles					
	0	1	2	3	4	5
cacc	100±0.0	98.9±0.7	91.2±1.5	82.4±4.7	73.0±3.6	59.8±3.3
npacc	99.8±0.4	95.9±2.0	84.4±2.7	77.8±2.6	59.2±3.2	57.2±1.5
sacc	95.8±2.9	84.3±2.6	71.4±6.9	70.6±5.2	68.7±5.1	63.9±0.7
zyc	42.6±10.3	42.4±6.5	39.2±3.2	38.2±2.3	36.0±2.8	35.8±1.5

Table 6. Comparison of adsorption capacity of previously reported adsorbents for methylene blue adsorption

Adsorbents	Adsorption capacity (mg g^{-1})	Reference
Commercial activated carbon composite film	146.8	This work
Nipa palm activated carbon composite film	123.6	This work
Sisal activated carbon composite film	103.7	This work
Ruthenium nanoparticle loaded activated carbon	94.6	[49]
Euphorbia rigida activated carbon powder	114.5	[50]
Wheat straw biochar powder	62.5	[51]
Luffa Actangula carbon powder	24.8	[52]
Activated carbon nanofiber (PAN based)	72.5	[53]
Clay	58.2	[54]
Tannin-immobilized cellulose microspheres	55.4	[48]
Freeze-dried agarose gel	10.4	[55]

sharing or exchanging of electrons between adsorbent and adsorbate [42]. We also noticed that k_2 of methylene blue adsorption of the zeolite composite (1.2883×10^{-3} g mg^{-1} min^{-1}), neat (7.6998×10^{-4} g mg^{-1} min^{-1}), commercial-ac composite (1.2016×10^{-4} g mg^{-1} min^{-1}), sisal-ac composite (8.8191×10^{-5} g mg^{-1} min^{-1}), nipa palm-ac composite (4.9282×10^{-5} g mg^{-1} min^{-1}) films was significantly different. This result indicated the adsorption rate of zeolite composite> neat>commercial-ac composite>sisal-ac composite>nipa palm-ac composite films.

The fitting curves of intraparticle diffusion model in Fig. S2, as well as calculated kinetics parameters in Table 4, revealed that the curves for all biocomposite films except the sisal-ac composite film were separated into two steps which did not pass through the starting point. Meanwhile, sisal-ac composite was divided into three parts. In the initial step for any films, methylene blue molecules in the aqueous solution were transferred onto the film surface (film diffusion). These dyes were then shifted and deposited into the pores within the biocomposite films (intraparticle diffusion) [32]. The third step, which happened only for sisal-ac composite, was the adsorptive attachment of dye particles [47]. Hence, this result suggested that the intraparticle diffusion was not the single rate-controlling step during the sorption process [48].

5. Reusability

The reusability of any adsorbent is an essential property to make the adsorption process become the cost-effective method for water treatment. The recycling of biocomposite films was studied by performing adsorption-desorption experiment and the % decolorization of each cycle was estimated as listed in Table 5. It was observed that the decolorization efficiency of the biocomposite films declined with increasing number of cycles and this could be attributed to the incomplete desorption of dye molecules. All of the biocomposite films in this study had a great adsorption efficiency and good reusability except zeolite composite film. The methylene blue removal efficiency was more than 70% up to three cycles, and still higher than 60% at the fifth cycle. Meanwhile, the % decolorization of zeolite composite was only 42.6% and declined to 35.8% after five cycles. The results indicate that the commercial-ac composite, nipa palm-ac composite, and sisal-ac composite are reusable adsorbents and still show good removal efficiency after being used several times.

The adsorption ability of other adsorbents for methylene blue dye removal was compared with the proposed commercial-ac composite, nipa palm-ac composite, and sisal-ac composite, as reported in Table 6. It is clearly shown that the adsorption capacity of biocomposite films in this work is better than the other previously reported works. Moreover, the convenience of recovery and isolation from effluent of the biocomposite films was one of the most outstanding features for this study. Therefore, it could be concluded that the currently prepared adsorbents are efficiently, economically, and practically feasible to be utilized as adsorbents for wastewater treatment.

6. Adsorption Mechanism

Several studies suggested that the adsorption of dye onto the adsorbent depended on numerous factors, including textural and surface properties of the adsorbent, chemical and structural characteristics of the adsorbate, and the adsorbate-adsorbent interactions during a sorption process [56]. After thorough analysis, the adsorption of cationic methylene blue dye by biocomposite films can occur through H-bonding interaction, π-π stacking interaction, electrostatic interaction, and van der Waals force or a simultaneous combination of those [57]. Hydrogen bonding is considered as one of the plausible mechanisms for dye adsorption; it can be

formed between H atoms within the biocomposite films and N atoms in the methylene blue molecules [58]. The aromatic-aromatic or π-π stacking interaction is another possible mechanism that can explain the sorption phenomenon. Since methylene blue contains benzene rings, it can generate the π-π stacking interaction with activated carbon because this porous material has a benzene ring as well [59]. Electrostatic interaction is also another essential driving force for the adsorption of methylene blue. This attractive force can occur between methylene blue cation and the negatively charged spots on the biocomposite film surface [60]. Therefore, it can be concluded that these interactions effectively enhance and play a crucial role in the sorption process of cationic methylene blue dye onto the surface of biocomposite films. Nevertheless, it seems that zeolite composite lacks π-π stacking interactions since both cellulose and zeolite do not have the benzene ring. Besides the morphology, the adsorption mechanism can also ascribe a low sorption capacity of zeolite towards methylene blue dye.

CONCLUSIONS

Biocomposite films were successfully fabricated by simple solution casting. Different fillers were embedded in regenerated cellulose matrix. The biocomposite film containing commercial activated carbon showed the highest capacity of approximately 146.81 mg g^{-1} for cationic methylene blue dye adsorption. Although the adsorption efficiency of nipa palm and sisal activated carbon composite was less than the biosorbent film with commercial activated carbon, the prepared activated carbon still possessed great adsorption ability and may be used in place of commercial one. The acquired adsorption isotherms of the commercial-ac composite and sisal-ac composite were fitted with the Langmuir model, while nipa plam-ac composite and zeolite composite were best described by Freundlich model. The adsorption kinetics data for all biocomposite films were well explained by the pseudo-second-order kinetic model, and the intraparticle diffusion model revealed that intraparticle diffusion was not the sole rate-limiting step. The reusability study showed that the biocomposite films can be regenerated five times and effectively utilized as a good reusable adsorbent for the treatment of cationic dye-contaminated wastewater.

ACKNOWLEDGEMENTS

The authors would like to acknowledge the 90th Anniversary of Chulalongkorn University Fund (Ratchadaphiseksomphot Endowment Fund [GCUGR1125622061D]) for financial support. One of the authors, N.S., would like to thank the scholarship from Science Achievement Scholarship of Thailand (SAST).

CONFLICT OF INTEREST

The authors declare that they have no conflict of interest.

SUPPORTING INFORMATION

Additional information as noted in the text. This information is available via the Internet at http://www.springer.com/chemistry/journal/11814.

REFERENCES

1. Y. Du and P. Zheng, *Korean J. Chem. Eng.*, **31**, 2051 (2014).
2. Q. Huang, M. Liu, J. Chen, K. Wang, D. Xu, F. Deng, H. Huang, X. Zhang and Y. Wei, *J. Mater. Sci.*, **51**, 8116 (2016).
3. M. Song, Z. Duan, R. Qin, X. Xu, S. Liu, S. Song, M. Zhang, Y. Li and J. Shi, *Korean J. Chem. Eng.*, **36**, 869 (2019).
4. Q. Li, Y. Zhao, L. Wang and W. Aiqin, *Korean J. Chem. Eng.*, **28**, 1658 (2011).
5. A. A. Sabri, T. M. Albayati and R. A. Alazawi, *Korean J. Chem. Eng.*, **32**, 1835 (2015).
6. A. K. Bhakta, S. Kumari, S. Hussain, P. Martis, R. J. Mascarenhas, J. Delhalle and Z. Mekhalif, *J. Mater. Sci.*, **54**, 200 (2019)
7. K. Mahmoudi, K. Hosni, N. Hamdi and E. Srasra, *Korean J. Chem. Eng.*, **32**, 274 (2015).
8. G. Zhu, X. Xing, J. Wang and X. Zhang, *J. Mater. Sci.*, **52**, 7664 (2017).
9. Y. Zhou, L. Zhang and Z. Cheng, *J. Mol. Liq.*, **212**, 739 (2015).
10. T. Kan, V. Strezov and T. J. Evans, *Renew. Sustain. Energy Rev.*, **57**, 1126 (2016).
11. Y. Shen, *Renew. Sustain. Energy Rev.*, **43**, 281 (2015).
12. X. Cui, H. Hao, Z. He, P. J. Stoffella and X. Yang, *J. Environ. Manage.*, **173**, 95 (2016).
13. Y. Lee, J. Park, C. Ryu, K. S. Gang, W. Yang, Y. K. Park, J. Jung and S. Hyun, *Bioresour. Technol.*, **148**, 196 (2013).
14. E. Agrafioti, G. Bouras, D. Kalderis and E. Diamadopoulos, *J. Anal. Appl. Pyrolysis*, **101**, 72 (2013).
15. S.-H. Kong, S.-K. Loh, R. T. Bachmann, S. A. Rahim and J. Salimon, *Renew. Sustain. Energy Rev.*, **39**, 729 (2014).
16. F. Nestler, L. Burhenne, M. J. Amtenbrink and T. Aicher, *Fuel Process. Technol.*, **145**, 31 (2016).
17. J. Tang, W. Zhu, R. Kookana and A. Katayama, *J. Biosci. Bioeng.*, **116**, 653 (2013).
18. A. Trubetskaya, P. A. Jensen, P. D. Jensen, M. Steibel, H. Spliethoff and P. Glarborg, *Fuel Process. Technol.*, **140**, 205 (2015).
19. A. Trubetskaya, P. A. Jensen, P. D. Jensen, A. D. G. Llamas, K. Umeki and P. Glarborg, *Fuel Process. Technol.*, **143**, 118 (2016).
20. J. J. Manya, F. X. Roca and J. F. Perales, *J. Anal. Appl. Pyrolysis*, **103**, 86 (2013).
21. P. Satyamurthy and N. Vigneshwaran, *Enzyme Micro. Technol.*, **52**, 20 (2013).
22. T. Lin, E. Goos and U. Riedel, *Fuel Process. Technol.*, **115**, 246 (2013).
23. C. Miao and W. Y. Hamad, *Cellulose*, **20**, 2221 (2013).
24. M. Ghaderi, M. Mousavi, H. Yousefi and M. Labbafi, *Carbohydr. Polym.*, **104**, 59 (2014).
25. T. Pullawan, A. N. Wilkinson and S. J. Eichhorn, *J. Mater. Sci.*, **48**, 7847 (2013).
26. N. Soykeabkaew, N. Arimoto, T. Nishino and T. Peijs, *Compos. Sci. Technol.*, **68**, 2201 (2008).
27. N. Somsesta, V. Sricharoenchaikul and D. Aht-Ong, The 10th International Conference on Materials Science and Technology, Bangkok, Thailand (2018).
28. V. O. Njoku, K. Y. Foo, M. Asif and B. H. Hameed, *Chem. Eng. J.*, **250**, 198 (2014).

29. C. Lu, C. Liu and G. P. Rao, *J. Hazard. Mater.*, **151**, 239 (2008).
30. A. O. Dada, A. P. Olalekan, A. M. Olatunya and O. Dada, *J. Appl. Chem.*, **3**, 38 (2012).
31. M. Li, Z. Wang and B. Li, *Desalination Water Treat.*, **57**, 16970 (2016).
32. X. Ma, C. Liu, D. P. Anderson and P. R. Chang, *Chemosphere*, **165**, 399 (2016).
33. P. Choeichom and A. Sirivat, *Ionics*, **24**, 2829 (2018).
34. S. Das, S. P. Mahanta and K. K. Bania, *RSC Adv.*, **4**, 51496 (2014).
35. T. H. Liou, *Chem. Eng. J.*, **158**, 129 (2010).
36. N. Salahudeen, A. S. Ahmed, M. Dauda, S. M. Waziri, B. Y. Jibril and A. H. Al Muhtaseb, *Aust. J. Ind. Res.*, **1**, 10 (2014).
37. L. Muniandy, F. Adam, A. R. Mohamed and E. P. Ng, *Micropor. Mesopor. Mater.*, **197**, 316 (2014).
38. V. Hospodarova, E. Hospodarova and N. Stevulova, *Am. J. Anal. Chem.*, **9**, 303 (2018).
39. K. Nakasone, S. Ikematsu and T. Kobayashi, *Ind. Eng. Chem. Res.*, **55**, 30 (2016).
40. C. Qin, N. Soykeabkaew, N. Xiuyuan and T. Peijs, *Carbohydr. Polym.*, **71**, 458 (2008).
41. G. Liu, Z. Hu, R. Guan, Y. Zhao, H. Zhang and B. Zhang, *Korean J. Chem. Eng.*, **33**, 3141 (2016).
42. L. Liu, Z. Y. Gao, X. P. Su, X. Chen, L. Jiang and J. M. Yao, *ACS Sustain. Chem. Eng.*, **3**, 432 (2015).
43. B. C. Melo, A. A. Francisco, A. A. Paulino, V. A. Cardoso, A. G. B. Pereira, A. R. Fajardo and F. H. A. Rodrigues, *Carbohydr. Polym.*, **181**, 358 (2018).
44. X. Luo and L. Zhang, *J. Hazard. Mater.*, **171**, 340 (2009).
45. Z. Zaheer, W. A. Bawazir, S. M. Al-Bukhari and A. S. Basaleh, *Mater. Chem. Phys.*, **232**, 109 (2019).
46. J. C. Igwe and A. A. Abia, *Ecl Quím*, **32**, 33 (2007).
47. H. N. Tran, S. J. You, A. H. Bandegharaei and H. P. Chao, *Water Res.*, **120**, 88 (2017).
48. Y. Pei, X. Wu, G. Xu, Z. Sun, X. Zheng, J. Liu and K. Tang, *J. Chem. Technol. Biotechnol.*, **92**, 1276 (2017).
49. S. Hajati, M. Ghaedi, B. Barazesh, F. Karimi, R. Sahraei, A. Daneshfar and A. Asghari, *J. Ind. Eng. Chem.*, **20**, 2421 (2014).
50. O. Gercel, A. Ozcan, A. S. Ozcan and H. Gercel, *Appl. Surf. Sci.*, **253**, 4843 (2007).
51. G. Li, W. Zhu, C. Zhang, S. Zhang, L. Liu, L. Zhu and W. Zhao, *Bioresour. Technol.*, **206**, 16 (2016).
52. S. H. Siddiqui, *Groundwat. Sustain. Dev.*, **6**, 141 (2018).
53. A. S. Ibupoto, U. A. Qureshi, F. Ahmed, Z. Khatri, M. Khatri, M. Maqsood, R. Z. Brohi and I. S. Kim, *Chem. Eng. Res. Des.*, **136**, 744 (2018).
54. A. Gürses, C. Dogar, M. Yalcın, M. Acıkyıldız, R. Bayrak and S. Karaca, *J. Hazard. Mater.*, **131**, 217 (2006).
55. W. Y. Seow and C. A. E. Hauser, *J. Environ. Chem. Eng.*, **4**, 1714 (2016).
56. S. Ghorai, A. Sarkar, M. Raoufi, A. B. Panda, H. Schönherr and S. Pal, *ACS Appl. Mater. Interfaces*, **6**, 4766 (2014).
57. I. Ali, M. Asim and T. A. Khan, *J. Environ. Manag.*, **113**, 170 (2012).
58. A. H. Jawad and A. S. Abdulhameed, *Surf. Interfaces*, **18**, 100422 (2020).
59. W. Konicki, M. Aleksandrzak, D. Moszynski and E. Mijowska, *J. Colloid Interface Sci.*, **496**, 188 (2017).
60. A. K. Prajapati and M. K. Mondal, *J. Mol. Liq.*, **307**, 112949 (2020).

Supporting Information

Adsorption isotherms and kinetics for the removal of cationic dye by *Cellulose*-based adsorbent biocomposite films

Noppon Somsesta[*], Chaichana Piyamawadee[*], Viboon Sricharoenchaikul[**], and Duangdao Aht-Ong[*,*,†]**

*Department of Materials Science, Faculty of Science, Chulalongkorn University, Bangkok, 10330, Thailand
**Department of Environmental Engineering, Faculty of Engineering, Chulalongkorn University, Bangkok, 10330, Thailand
***Center of Excellence on Petrochemical and Materials Technology, Chulalongkorn University, Bangkok, 10330, Thailand
(*Received 12 February 2020 • Revised 1 June 2020 • Accepted 4 June 2020*)

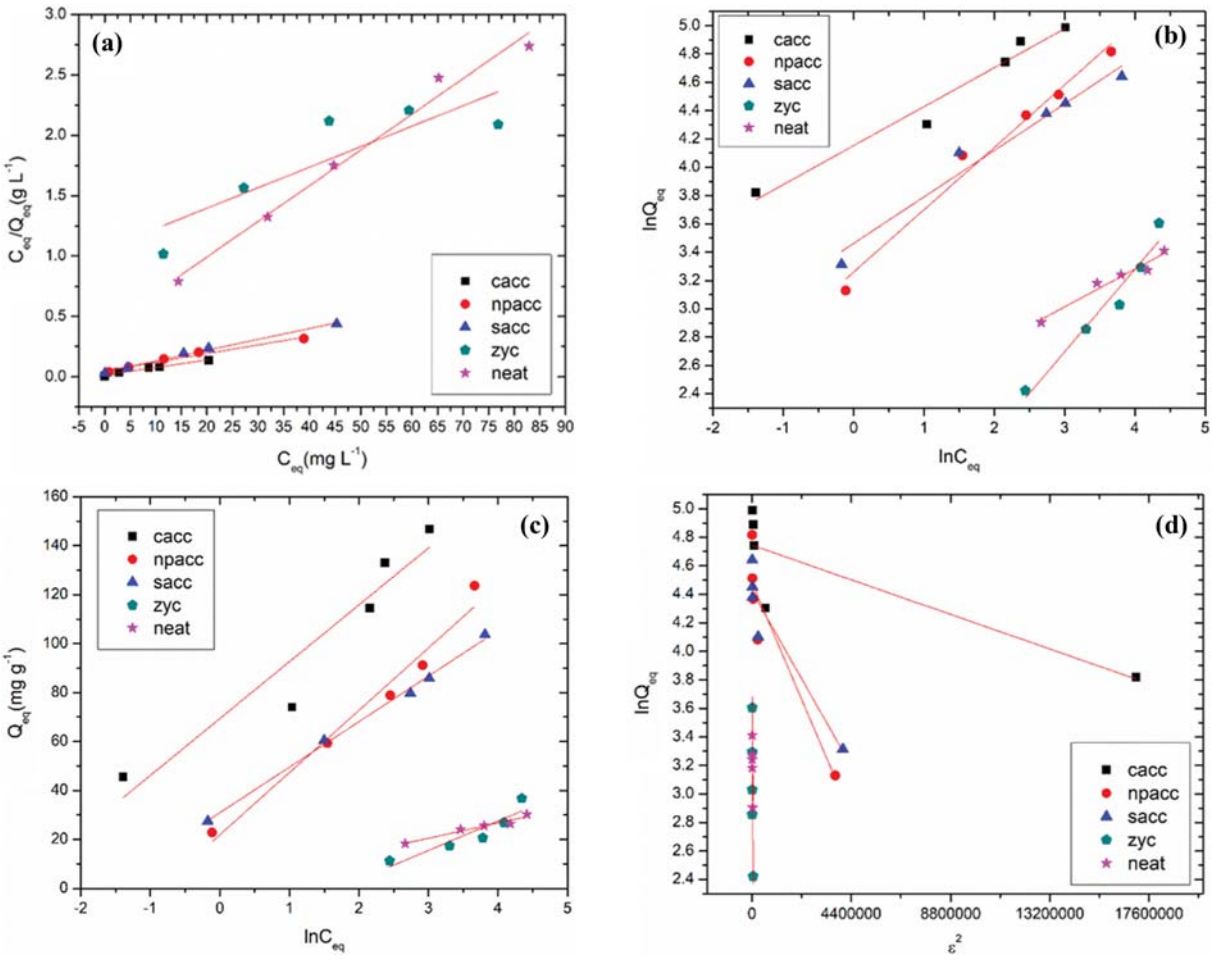

Fig. S1. Adsorption isotherm of methylene blue on cellulose neat, commercial activated carbon composite (cacc), nipa palm activated carbon composite (npacc), sisal activated carbon composite (sacc), and zeolite Y composite (zyc) films, (a) Langmuir isotherm, (b) Freundlich isotherm, (c) Temkin isotherm, (d) Dubinin-Raduskevich isotherm.

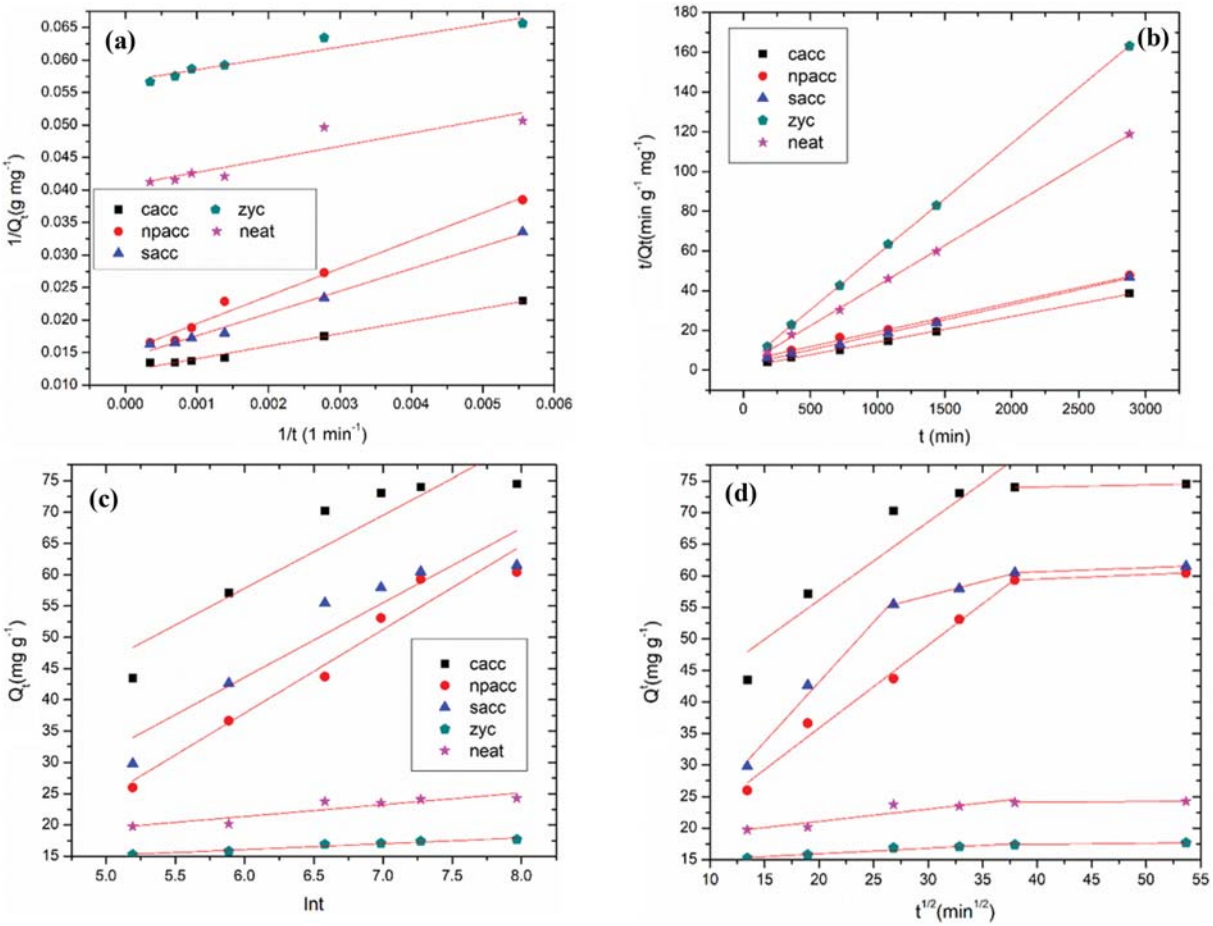

Fig. S2. Adsorption kinetic of methylene blue on cellulose neat, commercial activated carbon composite (cacc), nipa palm activated carbon composite (npacc), sisal activated carbon composite (sacc), and zeolite Y composite (zyc) films, (a) Lagergren pseudo-first order, (b) pseudo-second order, (c) Elovich, (d) intraparticle diffusion.